SPANDIDOS PUBLICATIONS

ONCOLOGY LETTERS 27: 24, 2024

Exosome-delivered miR-486-3p inhibits the progression of osteosarcoma via sponging CircKEAP1/MARCH1 axis components

HUIDONG YANG[1,2*], CHENG HE[3*], YI FENG[1] and JIE JIN[1]

[1]Department of Orthopedics, Wuhan Asia General Hospital Affiliated to Wuhan University of Science and Technology; [2]Department of Orthopedics, Wuhan University of Science and Technology School of Medicine, Wuhan, Hubei 430022; [3]Department of Orthopedics, The 908th Hospital of Joint Logistics Support Forces of Chinese PLA, Nanchang, Jiangxi 330002, P.R. China

Received January 27, 2023; Accepted September 26, 2023

DOI: 10.3892/ol.2023.14157

Abstract. Accumulating evidence shows that the disruption of competing endogenous RNA (ceRNA) networks plays a significant role in osteosarcoma (OS) initiation and progression. However, the specific roles and functions of the ceRNAs in OS remain unclear. First, differentially expressed microRNAs (DEMs) were identified by mining the E-MTAB-1136 and GSE28423 datasets. MiRWalk website was used to predict the target gene of miRNA. OS-associated circular RNA (circRNA) expression profiles were downloaded from the published microarray databases. Gene expression levels were assessed through reverse transcription-quantitative PCR and western blotting. The biological effects of circKEAP1, microRNA (miR)-486-3p and membrane-associated RINGCH finger protein 1 (MARCH1) in OS cells were investigated using Cell Counting Kit-8, Transwell, colony formation and wound healing assays. miR-486-3p was aberrantly downregulated in OS tissues and cell lines and was packed with exosomes. miR-486-3p overexpression was shown to inhibit OS cell progression and promoted cell cycle arrest *in vitro*. In addition, MARCH1 was identified as a direct downstream molecule of miR-486-3p in OS cells. circKEAP1 was found to be upregulated in OS tissues and cells. circKEAP1 was found to have binding sites with miR-486-3p. Mechanistically, circKEAP1 positively regulated MARCH1 expression by sponging miR-486-3p. Exosomal miR-486-3p inhibited the progression of OS by sponging the circKEAP1/MARCH1 axis. These findings may provide a promising treatment approach for OS.

Correspondence to: Dr Jie Jin, Department of Orthopedics, Wuhan Asia General Hospital Affiliated to Wuhan University of Science and Technology, 753 Jinghan Road, Wuhan, Hubei 430022, P.R. China
E-mail: y594611147@163.com

[*]Contributed equally

Key words: osteosarcoma, circular KEAP1, microRNA-486-3p, membrane-associated RINGCH finger protein 1, competing endogenous RNAs, exosome

Introduction

Osteosarcoma (OS) is one of the most common primary malignancies of the bone in adolescents and children (1). During the last few decades, the wide use of resection surgery and addition of neoadjuvant chemotherapy have led to an increase in the 5-year survival rate of patients with OS to 60-70% (2,3). However, the survival rates of patients who experience distant metastasis or local recurrence are still far from satisfactory (3). Therefore, new treatment modalities need to be investigated in order to improve the survival of patients with OS.

MicroRNAs (miRNAs or miRs) are small non-coding RNA molecules 19-25 nucleotides in length that impede gene expression by binding to the 3'-untranslated region (UTR) of their target mRNAs (4,5). Currently, the dysregulation of miRNAs has been identified in several types of human solid tumors, including prostate cancer, breast cancer, gastric cancer hepatocellular carcinoma and glioblastoma (6-10). In addition, increasing evidence shows that miRNAs play important roles in various aspects of tumor biology, such as cell cycle, progression, apoptosis and metabolism (11-13). For instance, Xin *et al* (14) demonstrated that miR-519c was significantly downregulated in pancreatic cancer, in which this miRNA significantly suppressed cell migration and metabolism under hypoxic conditions. Ren *et al* (15) showed that miR-210-3p was significantly increased in bone metastatic prostate cancer, and that miR-210-3p silencing inhibited epithelial-mesenchymal transition, invasion and migration of prostate cancer cells. Despite advances in the field, few miRNAs have been fully investigated in OS.

Recently, increasing evidence reports that miRNA can also be regulated by other regulators (16). Circular RNAs (circRNAs) have been shown to competitively sponge miRNAs and diminish their suppression of target mRNAs (17,18), act as competing endogenous RNA (ceRNA) (17). Experimental results have underscored the key role of circRNAs acting as ceRNAs in tumor development and progression (19,20). To

the best of our knowledge, however, studies on the role and mechanism of circRNA and ceRNA in OS remain in their infancy.

The present study aimed to investigate the role of circKEAP1/miR-486-3p/MARCH1 axis in OS progression to provide understanding of the role of miR-486-3p in the pathogenesis of OS and provide novel insights into the molecular mechanisms and therapeutic targets for OS.

Materials and methods

Bioinformatics analysis. First, the raw OS circRNA [GSE140256 (21)], miRNA [E-MTAB-1136 (22) and GSE28423 (23)] and mRNA data [TARGET-OS (24) and GSE12865 (25)], and the corresponding clinical information were downloaded from the Gene Expression Omnibus (https://www.ncbi.nlm.nih.gov/geo/), The Cancer Genome Atlas (https://www.cancer.gov/ccg/research/genome-sequencing/tcga) and ArrayExpress (https://www.ebi.ac.uk/biostudies/arrayexpress) databases. The expression matrix was standardized according to the Robust Multichip Average (RMA) and Linear Models for Microarray data (LIMMA) algorithms (26). Next, the differentially expressed genes (DEGs) between experiment and control groups were identified using the DESeq2 package with the thresholds of logFC>1.3 [log(fold change)] and P<0.05 (27). The candidate molecules were identified by overlapping DEGs with predicted targets and visualized using the VennDiagram 1.7.3 package (cran.r-project.org/).

Cell culture and transfection. MNNG/HOS, U2OS and hFOB1.19 cells were obtained from the Cell Bank of the Type Culture Collection of Chinese Academy of Sciences (Beijing, China). The OS cell lines were cultured in Eagle's minimal essential medium (Gibco; Thermo Fisher Scientific, Inc.) with 10% FBS (Gibco; Thermo Fisher Scientific, Inc.). The hFOB 1.19 was maintained in DMEM/F-12 (Gibco; Thermo Fisher Scientific, Inc.) supplemented with 10% FBS and 0.3 mg/ml G418. The cell culture environment was maintained at 37˚C with 5% CO_2.

The OS cells were cultured in six-well plates at a concentration of $3x10^4$ cells per well. Lipofectamine® 3000 (Invitrogen; Thermo Fisher Scientific, Inc.) was used for the plasmids (5 ug/plate) and miRNA mimic (50 nM) or inhibitor (100 nM) transfection. Briefly, plasmid cloning DNA [wild-type (wt)], miR-486-3p inhibitor or mimic as well as the respective controls (Mut-Type/inhibitor-NC/mimic-NC) were first mixed with Opti-MEM (Invitrogen; Thermo Fisher Scientific, Inc.), incubated for 5 min, co-incubated with Lipofectamine® 3000 for 20 min and transfected into cells for 72 h at 37˚C. In the construction of overexpression vector, the CircKEAP1sequence was cloned into the pLC5-circ vector (Guangzhou Geneseed Biotech Co., Ltd. Cat: GS0108) and the full-length (wt) MARCH1 was cloned into pcDNA3.1 (Thermo Fisher Scientific, Inc.; cat: V79020), the corresponding empty carrier was used as a control. As for the knockdown vectors, lentivirus short hairpin RNA (shRNA, 20uM/L) MARCH1 sequences (shRNA-MARCH1#1) which were ligated into the plasmid of pGC-silencer-U6/Neo and scrambled control shRNA (shRNA-NC) were established and synthesized by Jimon Biotechnology (Shanghai) Co., Ltd. Cells were then harvested for a later experiment.

Reverse transcription-quantitative PCR (RT-qPCR). TRIzol® (Invitrogen; Thermo Fisher Scientific, Inc.) was used to isolate total RNA. Reverse transcription was performed using the PrimeScript™ RT Reagent kit (Takara Bio, Inc.), and the First Strand cDNA Synthesis kit for miRNA (Sangon Biotech Co., Ltd.) was used according to the manufacturer's instructions. SYBR® Premix Ex Taq (Takara Bio, Inc.) was used for RT-qPCR on an Applied Biosystems StepOne-Plus Real-time PCR System, according to the manufacturer's instructions. Thermocycling conditions of PCR cycling were as following: Activation of TaqMan at 95˚C for 10 min, and then 40 cycles of denaturation at 95˚C for 10 sec, and annealing/extension at 60˚C for 60 sec. β-Actin served as a control for cellular RNA and mRNA. The level of miRNA was normalized against the endogenous reference U6. Quantification was performed using the $2^{-\Delta\Delta Cq}$ method (28). Primer sequences are listed in Table SI.

Colony formation assay. Transfected OS cells were seeded into six-well plates at a density of $5x10^2$ cells/well. After 2 weeks of incubation at 37˚C, these plates were fixed by 10% formaldehyde at room temperature and stained with 0.5% crystal violet solution at room temperature. The colonies were defined as >50 cells/colony and images were captured using an inverted microscope (Olympus IX71; Olympus Corporation). The numbers of colonies was then counted and measured using ImageJ software (version 1.8.0.112; National Institutes of Health).

5-Ethynyl-2'-deoxyuridine (EdU) analysis. Cell proliferation was detected using the EdU assay kit (Guangzhou RiboBio Co., Ltd.). Briefly, cells were seeded into 96-well plates at a density of $1x10^4$ cells/well. The OS cells were then treated with culture medium containing 50 μM EdU reagent at 37˚C for 2 h, and fixed with 4% formaldehyde for 30 min at room temperature. The nuclei were stained with Hoechst 33342 (10 ug/ml; MedChemExpress; Cat: HY-15559). Finally, the results were photographed using a fluorescence microscope (Nikon Corporation), and the number of EdU-positive cells were quantified and analyzed.

Wound healing assay. The transfected cells were implanted into a six-well plate. When cells had reached 80% confluence, they were scratched with a 200-μl sterile plastic tip, followed by culture in 2% serum culture medium at 37˚C for 48 h. Images of cells were captured.

Transwell cell migration and invasion assays. Briefly, for cell migration assay, $2x10^4$ OS cells were suspended in 200 μl medium free of serum and added into the top chamber. A total of 500 μl culture medium containing 30% FBS was added into the lower chamber. A total of 24 h after incubation at 37˚C, the cells on the upper surface of the membrane were removed gently and fixed in 4% paraformaldehyde for 10 min at room temperature. Next, 0.5% crystal violet was used to stain these cells for 20 min at room temperature. Images of the migratory or invasive cells were captured and counted under

a light microscope. However, for cell invasion assay, the filter membranes were precoated with Matrigel (Corning, Inc.) at 37˚C for 30 min, and other steps were performed as described in the migration assay.

Nucleic acid electrophoresis and Sanger sequencing. PCR products were separated by electrophoresis on a 2% agarose gel and gels were cut and sent to Shanghai Sangon Bioengineering Co., Ltd. for sequencing following observation in a UV imaging system.

Western blotting. Cell lysate was extracted using RIPA buffer (cat. no. P0013B; Beyotime Institute of Biotechnology) and then quantified with BCA Protein Assay (cat. no. P0012; Beyotime Institute of Biotechnology). Proteins (30 μg/lane) were separated via 10% SDS-PAGE, transferred to PVDF membranes (Millipore Sigma), blocked with 5% non-fat milk for 2 h at room temperature and probed with anti-MARCH1 (cat. no. PA5-69223; 1:1,000; Invitrogen; Thermo Fisher Scientific, Inc.) and anti-β-actin (cat. no. 66009-1-Ig; 1:5,000; ProteinTech Group, Inc.) primary antibodies overnight at 4˚C. This was followed by incubation with rabbit anti-mouse horseradish peroxidase-conjugated secondary antibodies (cat. no. #58802; CST; 1/1,000) for 60 min at room temperature. Enhanced chemiluminescence (Pierce; Thermo Fisher Scientific, Inc.) was performed to visualize the band signals, which were collected using the ChemiDoc XRS molecular imager system (Bio-Rad Laboratories, Inc.).

Flow cytometry. Harvested cells were fixed in 75% ethanol for 8 h at 4˚C. The cells were then washed twice with cold phosphate-buffered saline and resuspended in propidium iodide (50 μg/ml)/ribonuclease A (RNaseA; 50 μg/ml)-mixed staining solution for 30 min. Finally, a Beckman Coulter FACSCalibur (BD Biosciences) flow cytometer with the FlowJo 10.6.2 software system (Tree Star, Inc.) was employed to detect and analyze apoptotic cells.

Dual-luciferase reporter gene assay. miR-486-3p binding sites on MARCH1 were predicted using miRWalk3.0. For miRNA target gene luciferase reporter assays, the promoter region of MARCH1 was synthesized and subcloned into the pGL3 vector (GeneCreate Biotech). A total of $1x10^5$ OS cells were planted in a 24-well plate and cultured for 24 h at 37˚C. The pGL3 reporter vector bearing wt or mutant (mut) MARCH1 was then transfected into OS cells using Lipofectamine® 3000 (Invitrogen; Thermo Fisher Scientific, Inc.). CircRNAs containing wild or mutant full length of CircKEAP1 binding to miR-486-3p were synthesized and cloned into psiCHECK2 vector (Promega Corporation). Subsequently, cells were transfected with miR-486-3p mimic, inhibitor or control. After 48 h of transfection at 37 ˚C, relative luciferase activity was analyzed using Dual Luciferase Reporter Assay System (Promega Corporation). *Renilla* luciferase activity was used for normalization.

RNA immunoprecipitation (RIP) assay. Anti-Flag (Flag-MARCH1) antibody (10 μl, cat. no. 14793, Cell Signaling Technology, Inc.) and anti-IgG antibodies (10 μl, cat. no. 8726S, Cell Signaling Technology, Inc.) were incubated with protein A+G beads at 4˚C for 1 h following the instructions provided with the RIP kit (cat. no. P0101; Geneseed Biotech Co., Ltd.). Briefly, 1 ml of Buffer A working solution containing 1% volume protease inhibitor and 1% volume RNase inhibitor was prepared before use. A total of $1x10^7$ OS cells were used for each IP reaction and added to 1 ml of the configured RIP lysis buffer. The lysate (5 mg/ml, 400 μl) was then centrifuged at 14,000 x g for 10 min at 4˚C. The resulting supernatant was incubated with the antibody-attached magnetic beads for 1 h at 4˚C. The product was obtained by centrifugation at 12,000 x g for 1 min at 4˚C. The captured RNAs and target protein were finally eluted and purified for RT-qPCR.

Exosome experiments. Culture medium was pre-cleared by filtration through a 0.22-μm filter (MilliporeSigma), and exosomes were collected using a high-speed centrifuge (100,000 x g) at 4˚C for >1 h. The following exosome isolation was performed according to the manufacturer's instructions (Invitrogen; Thermo Fisher Scientific, Inc.). NP100 nanopores (NanoSight NS500; Zetaview) of the measurement system were calibrated using particles of known size (CPC100 standard solution) and washed twice with PBS. The exosome sample was diluted 1,000 times with PBS and subsequently added to the nanopores for the recording and tracking of each visible particle (NTA, Nanoparticle tracking analysis). and the morphology was captured by electron microscopy. For exosomal RNA extraction, an equal number of exosomes pre-treated with RNase were used for RNA extraction. For the *in vitro* exosome treatment, 1 μg exosomes (collected from ~$5x10^6$ cells) were added to $2x10^5$ recipient cells. PKH26 (cat: HY-D1451) and GW4869 (Cat: HY-19363) were purchased from MedChemExpress. PKH26 (10 μM) was incubated with exosomes for 5 min at 37˚C to labels exosomes. GW4869 (20 uM) was incubated with cells for 30 min at 37˚C to inhibit the release of exosomes.

Statistical analysis. Data are presented as the mean ± SD and were analyzed using R language (4.0.2, cran.r-project.org/) and GraphPad Prism 8.0 software (GraphPad Software, Inc.; Dotmatics). Unless otherwise specified, all experiments were performed at least three times. An unpaired t-test was used to estimate the statistical differences between two groups. One-way analysis of variance was used to determine the differences between three or more groups and followed by Tukey's post hoc test. The data met the assumptions of the tests. An estimate of variance was performed within each group of data. The variation is similar between the groups. $P<0.05$ was considered to indicate a statistically significant difference.

Results

miR-486-3p is aberrantly downregulated in OS tissues and cells. First, a total of 6 differentially expressed microRNAs (DEMs) were identified by overlapping analysis of OS-related datasets from the published microarray data (E-MTAB-1136 and GSE28423; Fig. 1A). As shown in the volcano plot, these DEMs were significantly downregulated in tumor tissue compared with that in normal tissues (Fig. 1B and C). Next, the expression level of these DEMs was investigated in OS cell lines and tissues. Of note, only miR-486-3p was significantly downregulated in OS cell lines (MNNG/HOS and U2OS), as

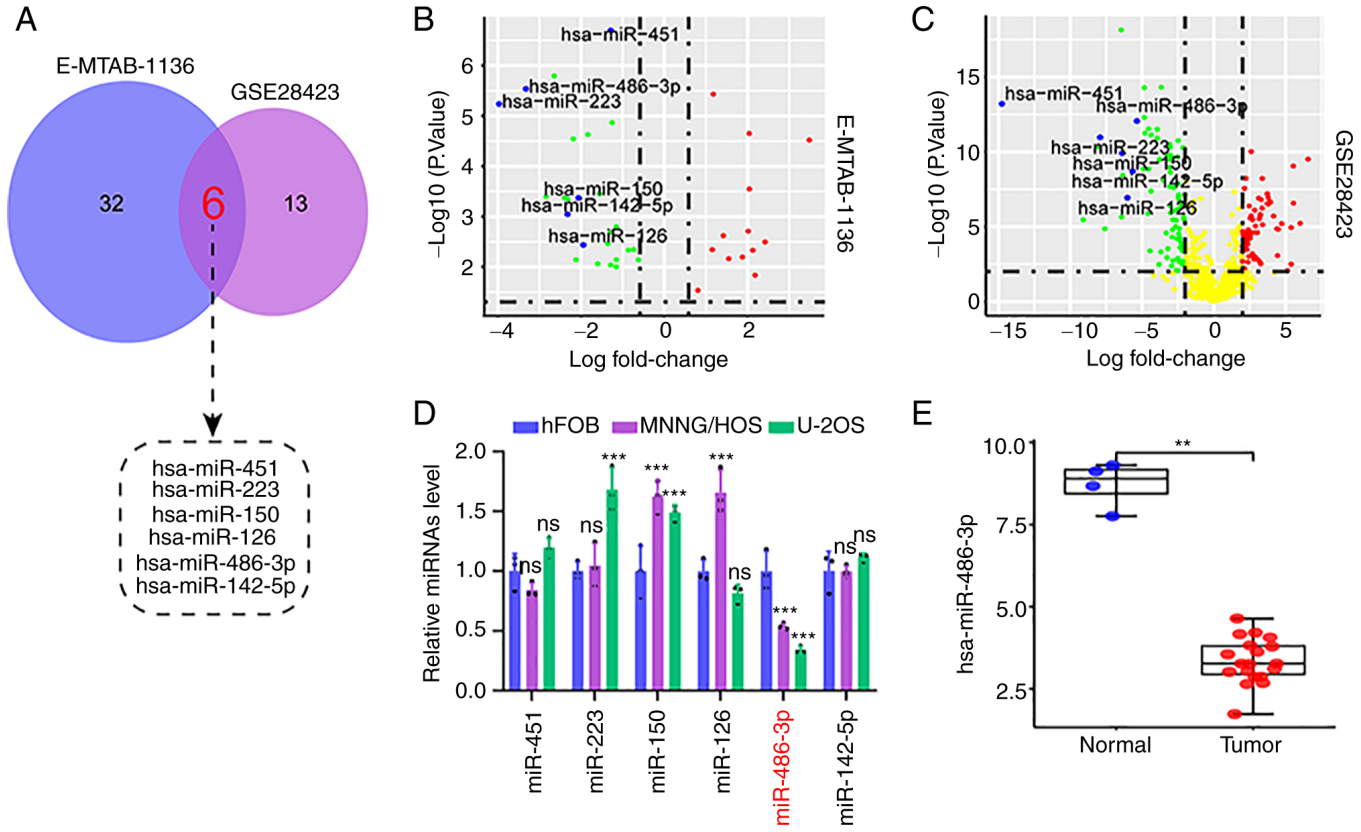

Figure 1. MiR-486-3p is downregulated in OS tissues and cells. (A) Venn diagram showed the DEMs in OS tissue using bioinformatics analysis based on E-MTAB-1136 and GSE28423 microarray datasets. (B) Volcano plot of 6 DEMs mined from E-MTAB-1136 dataset. (C) Volcano plot of 6 DEMs mined from GSE28423 dataset. (D) Reverse transcription-quantitative PCR analysis of the 6 DEMs in MNNG/HOS, U2OS and hFOB1.19 cells. (E) The expression level of miR-486-3p level in the OS tissues compared with para-normal tissue in GSE28423. miR, microRNA; OS, osteosarcoma; DEMs, differentially expressed microRNAs. **P<0.01, ***P<0.001.

compared with normal osteoblast cells (hFOB1.19; Fig. 1D); these findings were consistent with those in OS tissues from the GSE28423 dataset (Fig. 1E). These results suggested that miR-486-3p downregulation may play a key role in the occurrence and progression of OS.

miR-486-3p overexpression inhibits the progression of OS cells. To further investigate the biological effect of miR-486-3p, miR-486-3p mimics or inhibitors were transfected into MNNG/HOS and U2OS cells to upregulate or downregulate miR-486-3p expression. As shown in Fig. 2A, the transfection efficiency yielded a satisfactory result. The colony formation and EdU incorporation assays indicated that miR-486-3p overexpression inhibited MNNG/HOS and U2OS cell proliferation, and miR-486-3p silencing significantly promoted cell proliferation in these two cell lines (Fig. 2B and C). Moreover, Transwell invasion assay demonstrated that miR-486-3p overexpression significantly impeded MNNG/HOS and U2OS cell migration (Fig. 2D) and invasion (Fig. 2E). In addition, the wound healing assay demonstrated that miR-486-3p overexpression could significantly inhibit OS cell migration (Fig. 3A). The cell cycle was analyzed by flow cytometry and the results showed that the percentage of OS cells in S phase was reduced in the miR-486-3p mimic group (Fig. 3B), suggesting that miR-486-3p overexpression halted the cell cycle in the G1/S transition. Comparatively, miR-486-3p deficiency produced the reverse effect in MNNG/HOS and U2OS cells. In combination, these data suggested that miR-486-3p overexpression can delay the progression of OS cells.

MARCH1 is a direct target of miR-486-3p. To improve understanding of the underlying mechanisms of miR-486-3p, the bioinformatics datasets TARGET-OS, GSE12865 and miRWalk3.0 database were searched to predict potential target genes of miR-486-3p, as previously reported (29-32). As demonstrated in the Venn diagram, a total of eight genes were identified as the underlying target of miR-486-3p (Fig. 4A). Among them, five genes (PDE10A, THRB, UNC5C, MARCH1 and ROBO2) were simultaneously upregulated in OS samples compared with the non-cancerous samples, as shown in the volcano plots (Fig. 4B and C). The expression levels of these genes in OS cells were analyzed using RT-qPCR. As compared with the hFOB1.19 cells, only MARCH1 expression was elevated in both OS cells (Fig. 4D). Furthermore, a significantly decreased expression of MARCH1 following miR-486-3p overexpression was identified in MNNG/HOS and U2OS cells (Fig. 4E). The MARCH1 mRNA was found to have potential binding sites for miR-486-3p (Fig. 4F). Next, the luciferase reporter assay was carried out to validate their binding, and it was observed that the co-transfection of the wt MARCH1 vector (Luc-MARCH1-wt) and miR-486-3p mimics, but not the mut MARCH1 vector (Luc-MARCH1-mut), significantly suppressed luciferase activity in MNNG/HOS and

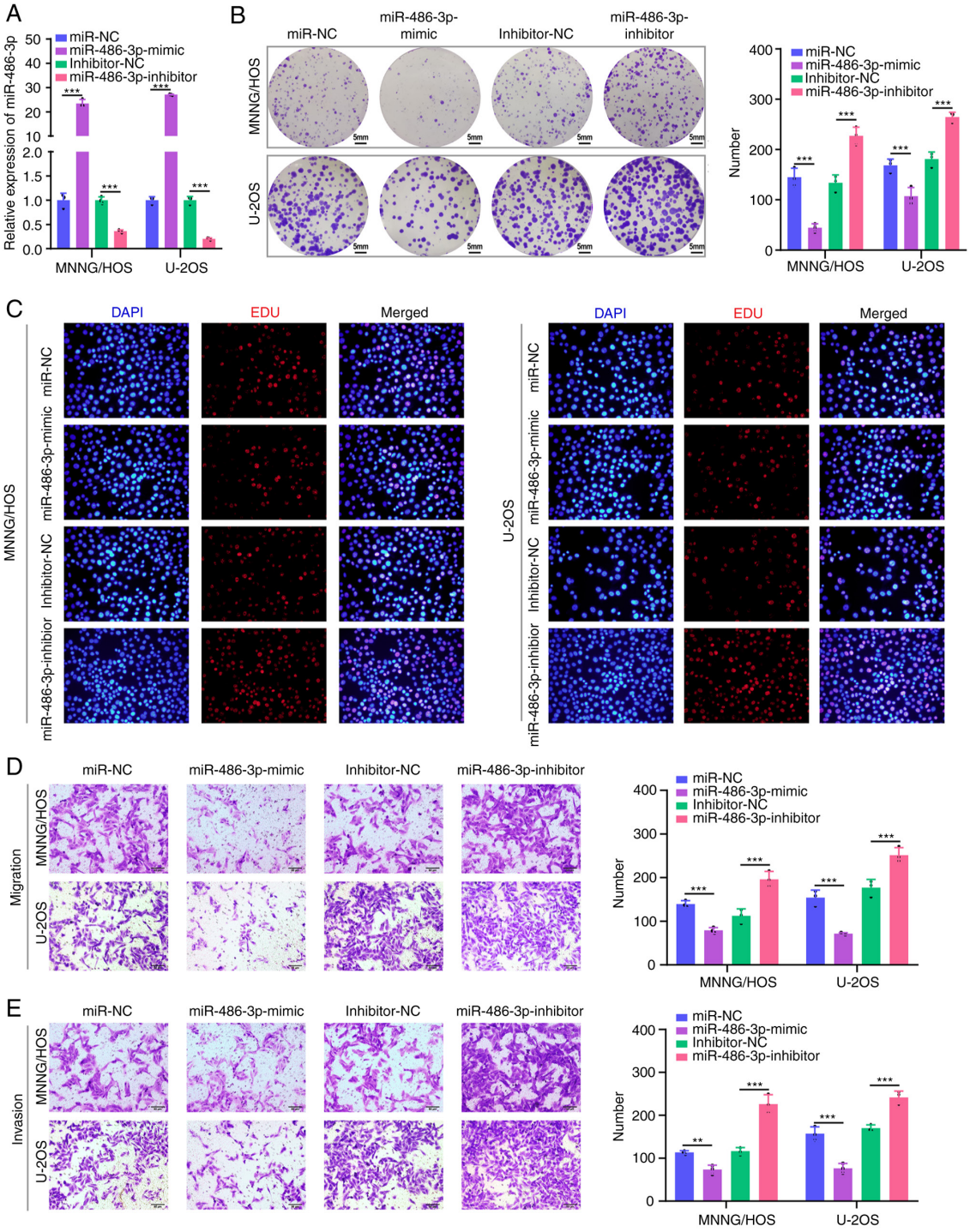

Figure 2. miR-486-3p overexpression inhibits the progression of osteosarcoma cells. (A) Reverse transcription-quantitative PCR analysis of miR-486-3p expression with miR-486-3p overexpression or miR-486-3p knockdown in MNNG/HOS and U2OS cells. (B) Cell proliferative ability was measured by colony formation with miR-486-3p overexpression or miR-486-3p knockdown in MNNG/HOS and U2OS cells. (C) EdU incorporation assays were performed to assess the cell proliferation ability. (D and E) Transwell assay was exploited to explore the invasive and migratory ability with miR-486-3p mimics or miR-486-3p inhibitors in MNNG/HOS and U2OS cells. miR, microRNA; EdU, 5-Ethynyl-2'-deoxyuridine; NC, negative control. **P<0.01, ***P<0.001.

U2OS cells (Fig. 4G). RIP experiments also proved that they are bond with each other (Fig. 4H). Therefore, MARCH1 was the downstream target gene of miR-486-3p in OS.

MARCH1 overexpression in MNNG/HOS and U2OS cells increased the colony numbers, an affect that could be largely attenuated by miR-486-3p mimic transfection (Fig. 4I). The same trend as that of cell proliferation was observed in EdU incorporation experiments (Fig. 4J). Similarly, the overexpression of miR-486-3p could reverse the increase in cell migration and invasion caused by MARCH1 overexpression (Fig. 4K and L). Overall, the findings of the present study, indicated that miR-486-3p could suppress the progression of OS cells by targeting MARCH1.

circKEAP1 directly targets miR-486-3p in OS cells. Accumulating evidence indicates that the ceRNA networks

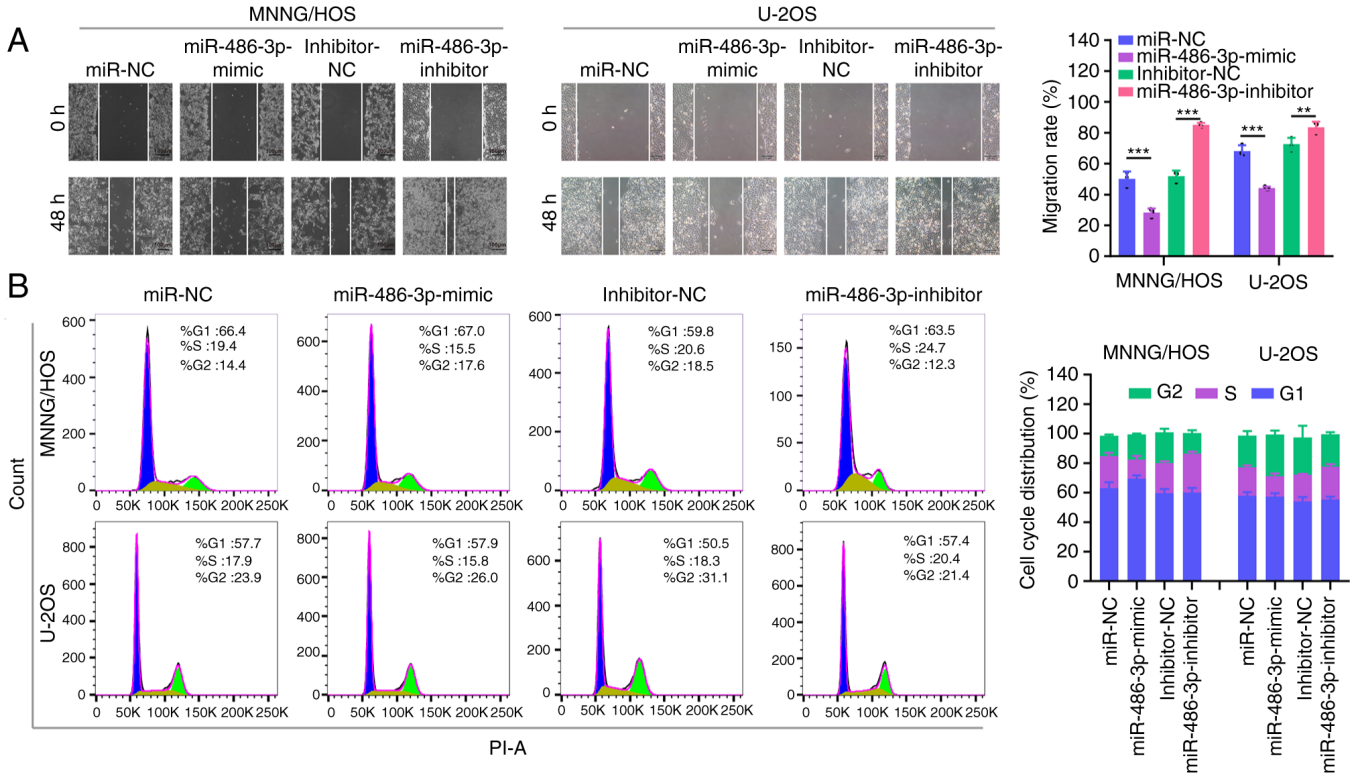

Figure 3. MiR-486-3p overexpression inhibits the migration and blocks cell cycle of osteosarcoma cells. (A) Cell mobility was evaluated by wound-healing assay with miR-486-3p overexpression or miR-486-3p knockdown in MNNG/HOS and U2OS cells. (B) Cell cycle was measured by flow cytometry analyses with miR-486-3p overexpression or miR-486-3p knockdown in MNNG/HOS and U2OS cells. miR, microRNA; NC, negative control. **P<0.01, ***P<0.001.

play a significant role in the occurrence and progression of cancer (20). To investigate potential circRNAs that regulate miR-486-3p expression in OS, differentially expressed circRNAs (DECs) from GSE140256 were overlapped with predicted targets from the circBank database. As a result, a total of four DECs (hsa_circ_0078767, hsa_circ_0010220, hsa_circ_0020378 and hsa_circ_0049271) were identified (Fig. 5A). Among them, two circRNAs were upregulated and two were downregulated in the OS samples compared with the non-cancerous samples, as shown in the volcano plot (Fig. 5B). Next, the expression level of these 4 DECs were determined in OS cell lines, and it was found that only hsa_circ_0049271 (circKEAP1) was validated by PCR amplification using divergent primers from the cDNA of OS cell lines (Fig. 5C). Hsa_circ_0049271 derived from the KEAP1 gene exon 2, and Sanger sequencing confirmed the head-to-tail splicing structure in circKEAP1 (Fig. 5D). In addition, the circular properties of circKEAP1 were also identified using divergent and convergent primers (Fig. 5E). circKEAP1 was also significantly upregulated in OS cells, as revealed by RT-qPCR (Fig. 5F). Of note, miR-486-3p overexpression decreased the expression of circKEAP1, while miR-486-3p silencing increased the expression of circKEAP1 in MNNG/HOS and U2OS cell lines (Fig. 5G). Moreover, dual luciferase reporter assay indicated a direct regulatory association between miR-486-3p and circKEAP1 (Fig. 5H).

To further explore the pathological role of circKEAP1 in OS cells, circKEAP1 overexpression vectors (circKEAP1-OE) were transfected into MNNG/HOS and U2OS cells. As compared with the blank control group, the expression level of circKEAP1 was significantly upregulated in both cell types following transfection with circKEAP1-OE (Fig. 5I). It was subsequently investigated whether circKEAP1 plays a tumor-promoting role by sponging miR-486-3p by co-transfecting MNNG/HOS and U2OS cells with miR-486-3p mimics and circKEAP1 overexpression vectors. circKEAP1 upregulation blocked the inhibition of cell proliferation, migration and invasion caused by miR-486-3p mimics (Fig. 5J-L). In combination, these results suggested that circKEAP1 can sponge miR-486-3p to affect OS cell proliferation, migration and invasion.

circKEAP1 promotes OS cell proliferation and migration through MARCH1 upregulation. To investigate whether circKEAP1 plays a promoting role in OS by upregulating MARCH1, sh-MARCH1 alone or combined with circKEAP1-OE plasmid was transfected into OS cells. As shown by the colony formation assay results, following circKEAP1 upregulation, the cell proliferation ability exhibited by the two OS cell lines was significantly increased, which was effectively reversed by MARCH1 downregulation (Fig. 6A). Similarly, EdU-positive cells were increased following circKEAP1-OE plasmid transfection, whereas following MARCH1 knockdown reversed this increase (Fig. 6B). Furthermore, the Transwell assay results revealed that MARCH1 knockdown could reverse the promoting effect of circKEAP1 overexpression on the invasion and migration ability of MNNG/HOS and U2OS cells (Fig. 6C and D). Collectively, these results suggested that circKEAP1 regulated MARCH1 expression by sponging miR-486-3p in OS cells.

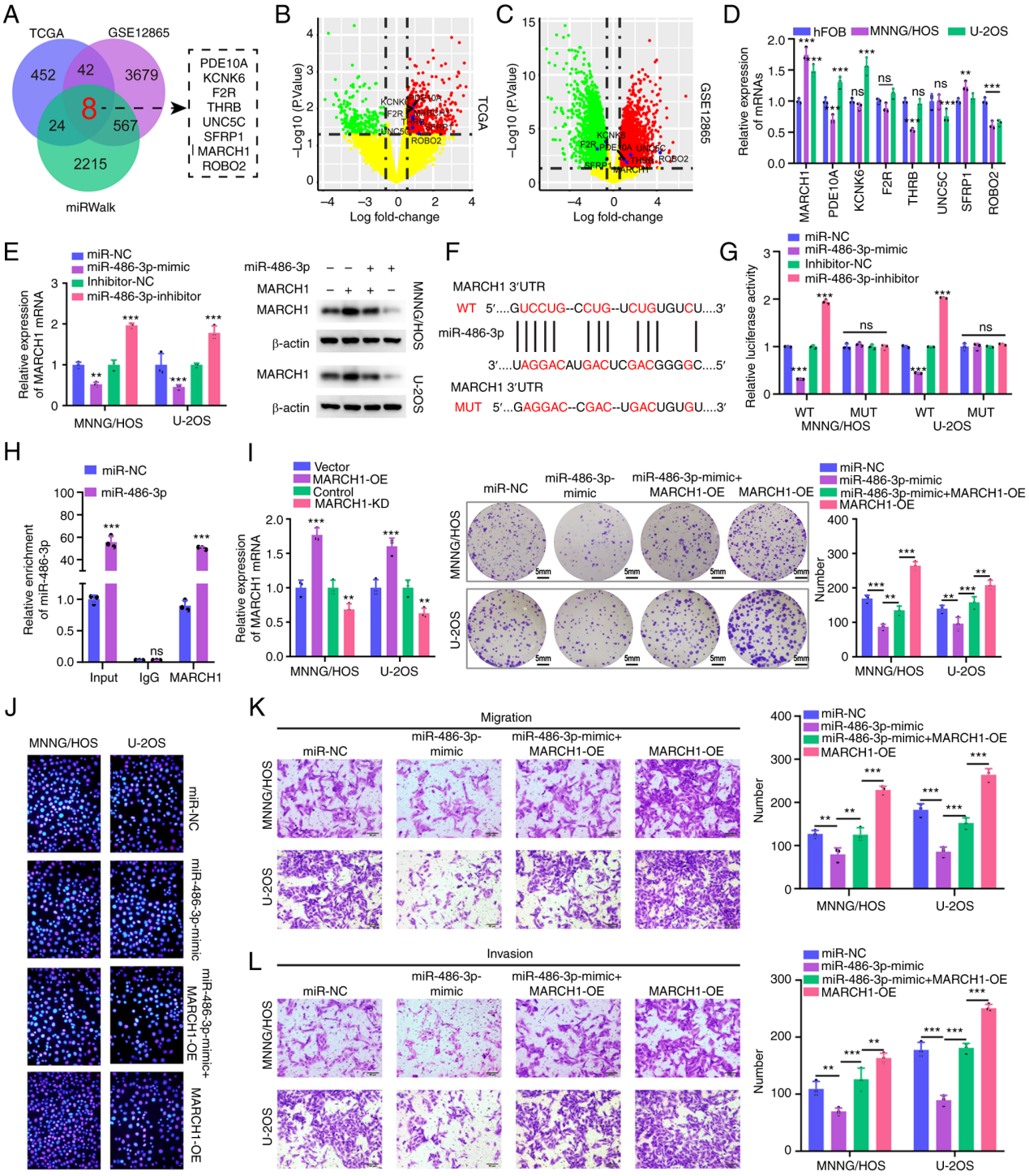

Figure 4. MARCH1 is a direct target of miR-486-3p. (A) Overlapping analysis of DEGs in osteosarcoma tissues using bioinformatics analysis based on TCGA, GSE12865 datasets as well as miRWalk database. (B and C) Volcano plot of the selected 8 DEGs in the TARGET-OS and GSE12865 datasets. (D) RT-qPCR analysis for 8 screened mRNAs in MNNG/HOS, U2OS and hFOB1.19 cells. (E) RT-qPCR and western blot assay were applied to evaluated MARCH1 mRNA (left) and protein level (right) in MNNG/HOS and U2OS cells with or without miR-486-3p mimics. (F) The binding sites of MARCH1 and miR-486-3p and the mutant sequence of MARCH1 based on binding region. (G) miR-486-3p mimics suppressed the luciferase activity of MARCH1 wt vector in MNNG/HOS and U2OS cells. (H) The enrichment level of IgG or MARCH1 to miR-486-3p was evaluated by RNA immunoprecipitation assay with or without miR-486-3p overexpression. (I and J) Cell proliferative ability was measured by colony formation and 5-Ethynyl-2'-deoxyuridine incorporation assays with MARCH1 overexpression or MARCH1 overexpression + miR-486-3p mimics in MNNG/HOS and U2OS cells. The transfection efficiency of vectors that overexpress and knock down MARCH1 was validated at 4I (left). (K and L) Transwell assay was exploited to explore the invasive and migratory ability with MARCH1 overexpression or MARCH1 overexpression + miR-486-3p mimics in MNNG/HOS and U2OS cells. MARCH1, membrane-associated RINGCH finger protein 1; miR, microRNA; DEG, differentially expressed genes; TCGA, The Cancer Genome Atlas; RT-qPCR, reverse transcription-quantitative PCR; wt, wild-type; mut, mutant; NC, negative control; OE, overexpression. **P<0.01, ***P<0.001.

Exosomal miR-486-3p reverses OS cell progression via packing into exosomes. The presence mode of extracellular miR-486-3p was examined to explore whether extracellular miR-486-3p regulates the progression of OS by packing into

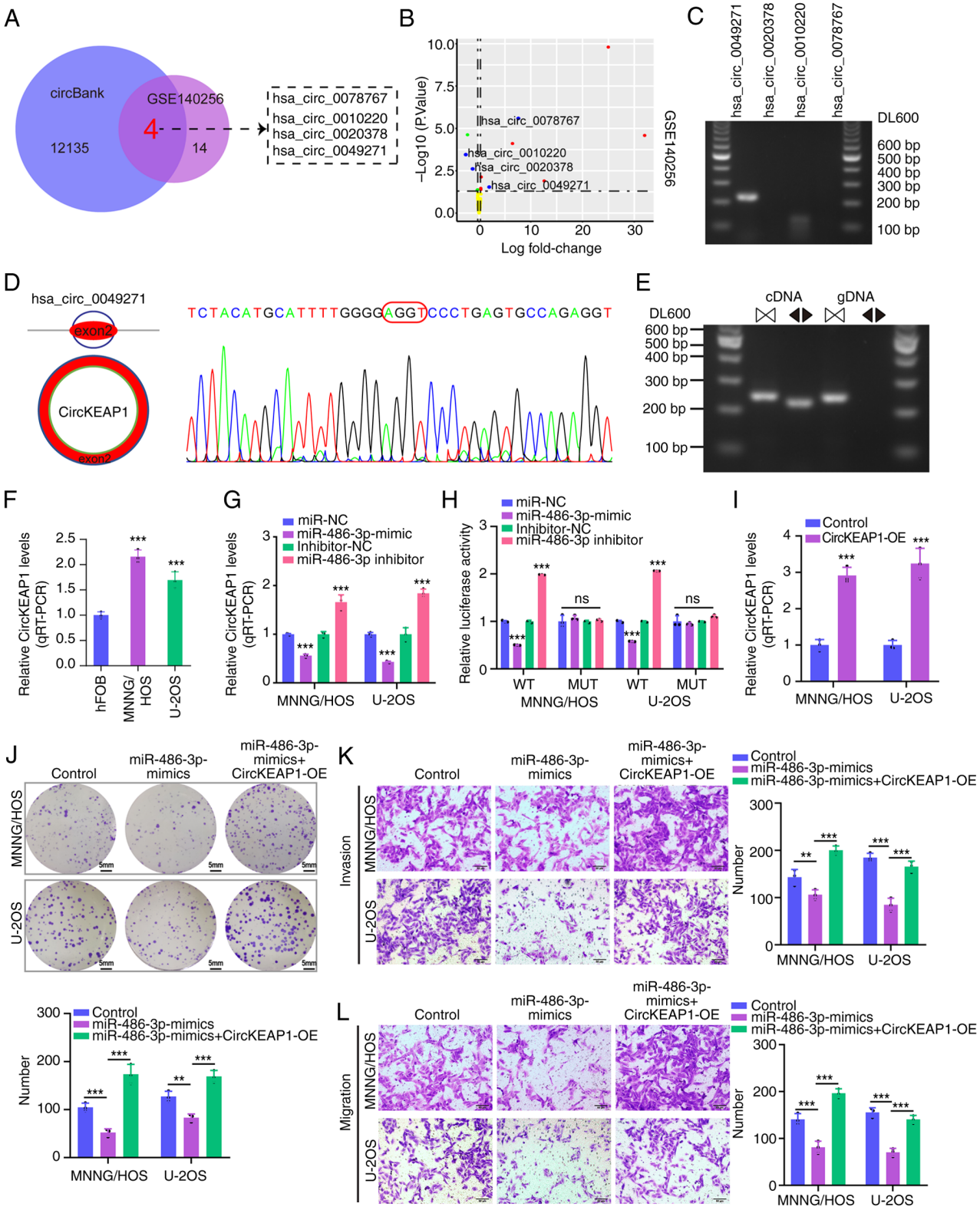

Figure 5. CircKEAP1 directly targets miR-486-3p in osteosarcoma cells. (A) DECs from GSE140256 dataset were overlapped with predicted target circRNAs from circBank database. (B) Volcano plot of the selected 4 DECs in the GSE140256 dataset. (C) The expression level of 4 screened DECs in MNNG/HOS cells. (D and E) The characterization of circKEAP1. The expression level of circKEAP1 was assessed via RT-qPCR assay and Sanger sequencing. Arrows represent divergent primers targeting circKEAP1 genome region (Left); RT-qPCR products using divergent primers indicating circularization of circKEAP1. cDNA represents complementary DNA. gDNA represents genomic DNA (Right). (F) RT-qPCR analysis of circKEAP1 expression in MNNG/HOS, U2OS and hFOB1.19 cells. (G) RT-qPCR analysis of circKEAP1 expression with miR-486-3p overexpression or miR-486-3p knockdown in MNNG/HOS and U2OS cells. (H) miR-486-3p mimics suppressed the luciferase activity of circKEAP1 wild-type vector in MNNG/HOS and U2OS cells. (I) RT-qPCR assays for investigation of circKEAP1 expression levels with circKEAP1 overexpression vectors in MNNG/HOS and U2OS cells and empty vector was used as negative control. (J) Cell proliferation was detected via colony formation with miR-486-3p mimics or miR-486-3p mimics + circKEAP1 overexpression in MNNG/HOS and U2OS cells. (K and L) Transwell assay was exploited to explore the invasive and migratory ability in MNNG/HOS and U2OS cells. DEGs, differentially expressed genes; circ, circular; miR, microRNA; DECs, differentially expressed circRNAs; RT-qPCR, reverse transcription-quantitative; gDNA, genomic DNA; NC, negative control; OE, overexpression. **P<0.01, ***P<0.001.

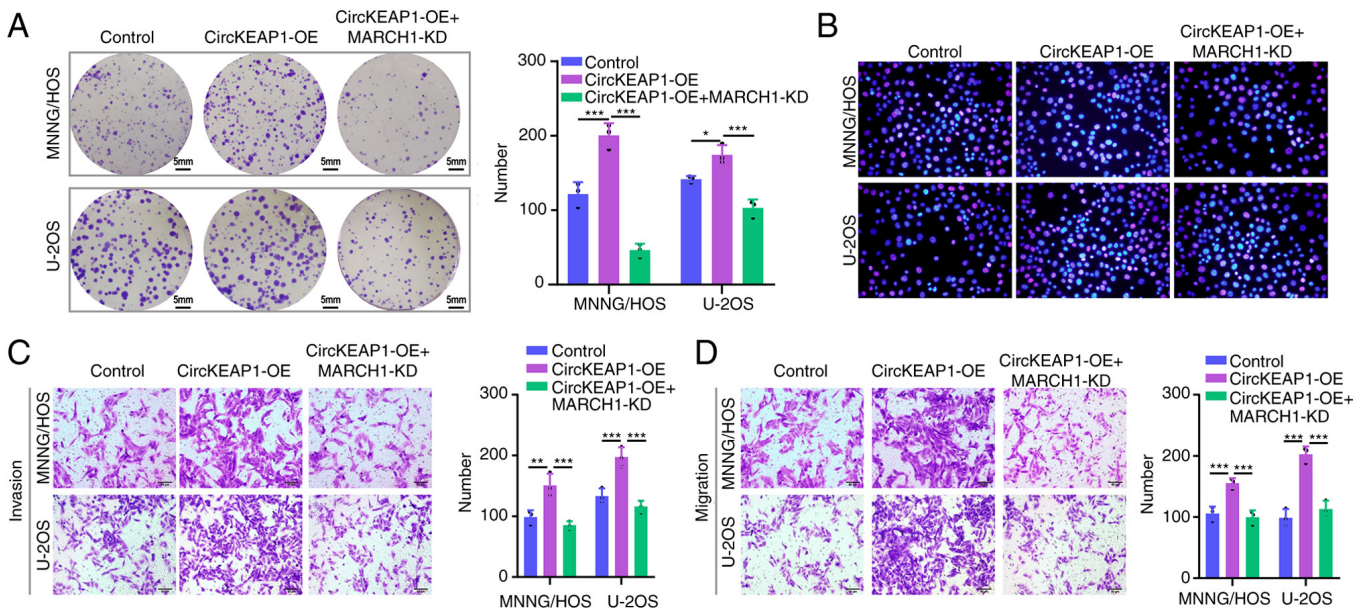

Figure 6. CircKEAP1 promotes cell proliferation and migration of osteosarcoma via upregulation of MARCH1. (A and B) Cell proliferation was detected via colony formation and 5-Ethynyl-2'-deoxyuridine incorporation assays with circKEAP1 overexpression or circKEAP1 overexpression + MARCH1 knockdown in MNNG/HOS and U2OS cells. (C and D) Transwell assay was exploited to explore the invasive and migratory ability with circKEAP1 overexpression or circKEAP1 overexpression + MARCH1 knockdown in MNNG/HOS and U2OS cells. circ, circular; MARCH1, membrane-associated RINGCH finger protein 1; OE, overexpression; KD, knockdown. *P<0.05, ***P<0.001.

exosomes. The level of miR-486-3p in the culture medium was not disturbed following RNase A treatment but was significantly reduced when Triton 100 and RNase A were treated simultaneously (Fig. 7A), demonstrating that miR-486-3p was wrapped with extracellular vesicles instead of being secreted directly. Next, exosomes were extracted from culture medium to verify this hypothesis. Nanoparticle tracking analysis revealed that the size of exosomes was 30-200 nm (Fig. 7B). In addition, exosome markers TSG101 and CD63 confirmed the identity of exosomes (Fig. 7C). In addition, the expression levels of extracellular miR-486-3p were almost equivalent to that of exosomal miR-486-3p (Fig. 7D), suggesting that extracellular miR-486-3p was mainly carried by exosomes. As revealed in Fig. 7E, exosomal miR-486-3p levels had a mostly high expression in culture medium from hFOB cells and low expression in culture medium from MNNG/HOS and U2OS cells. Next, it was further explored whether miR-486-3p-bearing exosomes were taken up by the recipient cells. First, exosomes were isolated from hFOB cells, labeled with PKH26 dye, and incubated with MNNG/HOS and U2OS cells for 48 h. A strong red signal in the recipient cells presented in Fig. 7F indicated exosome intake by recipient cells. miR-486-3p expression in exosomes derived from hFOB cells decreased significantly following transfection with miR-486-3p inhibitors (Fig. 7G). Following co-culture with exosomes derived from hFOB cells transfected with miR-486-3p mimics and inhibitors, the cell viability of MNNG/HOS and U2OS cells was significantly decreased and enhanced, respectively (Fig. 7H). Finally, it was explored whether exosomal miR-486-3p played a deterministic role. Exosome production was blocked using GW4869 (Fig. 7I and J). Incubation with culture medium from hFOB cells treated with GW4869 failed to influence the cell viability of MNNG/HOS and U2OS cells (Fig. 7K). In conclusion, the extracellular miR-486-3p inhibited OS cell viability through exosomes.

Discussion

OS is the most common primary malignancy of the bone, and its treatment remains far from satisfactory due to its high propensity for recurrence, local invasion and early metastasis (33). Emerging evidence has underscored the roles of mRNA-miRNA-circRNA network in tumorigenesis and tumor development (17,34). In the present study, a circRNA named circKEAP1 was found to be significantly increased in OS tissues. A function assay showed that circKEAP1 could act as a sponge for miR-486-3p to relieve the suppression of this miRNA for its target gene, MARCH1, in OS cells.

miRNAs play a major role in the pathogenesis of OS and various other types of cancer (35,36). Theoretically, mRNAs can bind to miRNAs and play a functional role in a ceRNA pattern (37). Recently, circRNAs acting as ceRNAs, have been reported to play important roles in miRNA sponges (38). In the present study, it was first shown that miR-486-3p was downregulated in OS tissues when compared with para-cancerous normal tissues. Similarly, miR-486-3p exhibited a low expression in OS cell lines, indicating the potential role of miR-486-3p in OS progression. Subsequent results indicated that the overexpression of miR-486-3p significantly suppressed cell proliferation, invasion and migration. An opposite trend was observed in OS cells with miR-486-3p knockdown. miR-486-3p can block the progression of OS cells and play a regulatory role in cancer growth, migration and invasion (39-41). However, the mechanisms explaining how miR-486-3p acts as a regulator during carcinogenesis and cancer progression have not been fully elucidated. In the present study, the bioinformatics analysis was

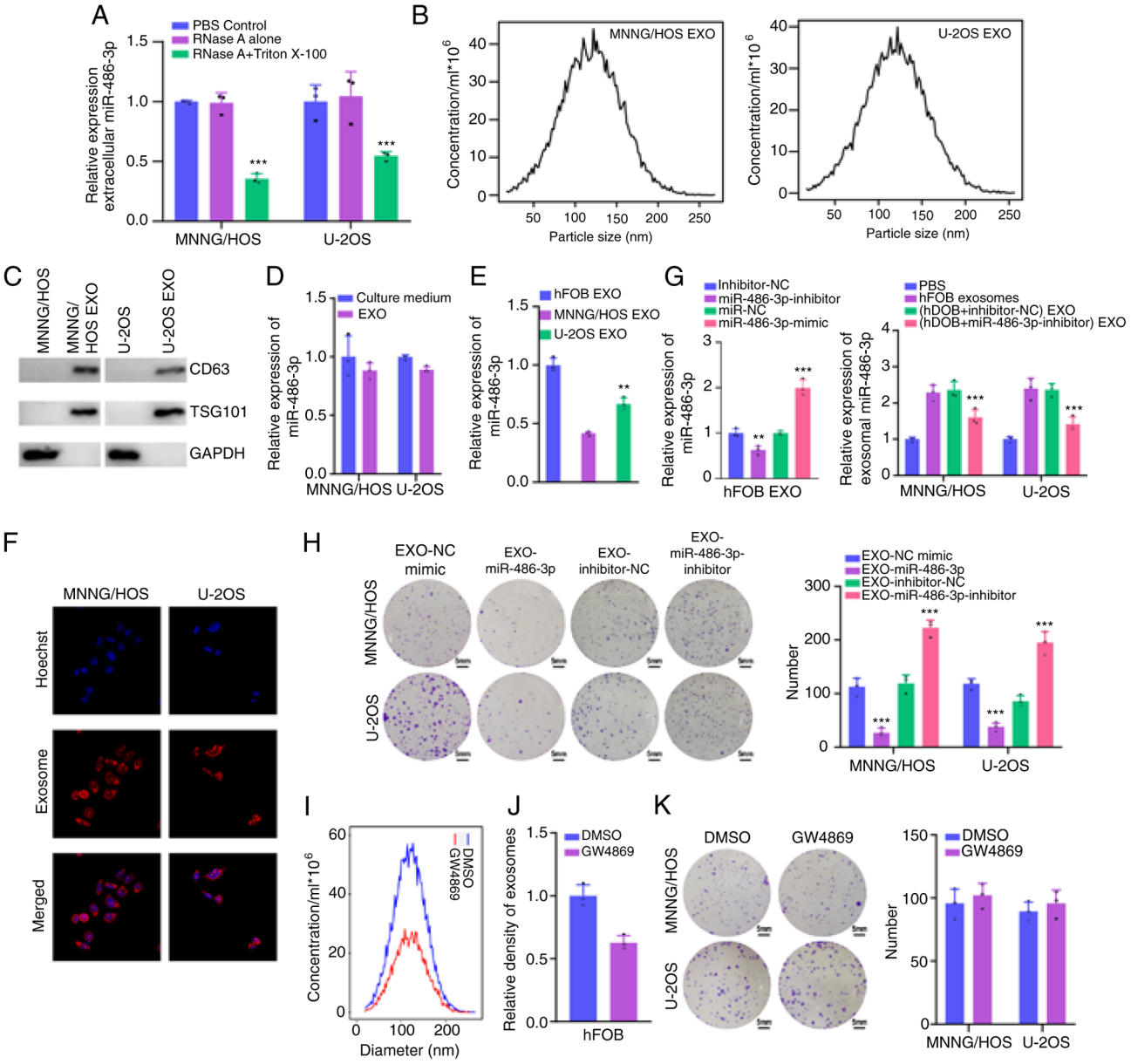

Figure 7. miR-486-3p inhibits osteosarcoma development through packaging into exosomes. (A) Extracellular miR-486-3p was degraded by treatment with RNase A and Triton simultaneously. (B) Size distribution of exosomes were analyzed by NTA. (C) Markers (TSG101 and CD63) of exosomes were analyzed by western blotting. (D) miR-486-3p expression in culture medium and exosomes was analyzed by RT-qPCR. (E) Exosomal miR-486-3p levels were analyzed by RT-qPCR. (F) Exosomes of hFOB were extracted and labeled with PKH26 dye followed by incubation with MNNG/HOS and U2OS cells. (G) The miR-486-3p expression level in hFOB cell exosomes was verified after transfection of miR-486-3p inhibitors or NC (left). The expression level of miR-486-3p in MNNG/HOS and U2OS cells co-cultured with hFOB cell exosomes or not was evaluated (Right). (H) Cell proliferation was determined using colony formation assay in MNNG/HOS and U2OS cells incubated with exosomes from hFOB cells transfected with miR-486-3p mimics or inhibitors. (I and J) The size distributions and number of exosomes from hFOB cells treated with GW4869 were analyzed by NTA. (K) Cell proliferation was determined using colony formation assay in MNNG/HOS and U2OS cells incubated with exosomes from GW4869-treated hFOB cells. **P<0.01 and ***P<0.001. miR, microRNA; NTA, nanoparticle tracking analysis; RT-qPCR, reverse transcription-quantitative; NC, negative controls

used to search for the downstream target of miR-486-3p, and the MARCH1 gene was finally screened out. Dual-luciferase reporter gene assay also confirmed the binding relationship between miR-486-3p and MARCH1.

MARCH1, as a member of the membrane-anchored E3 ubiquitin ligases (42), has been reported to be overexpressed in ovarian cancer, hepatocellular carcinoma and colorectal cancer, and its downregulation has been reported to contribute to cancer treatment (43-45). In addition, circRNA-6 has been shown to suppress bladder cancer growth by sponging miR-653 to regulate MARCH1 levels (46). In the present study, it was found that MARCH1 was highly expressed in OS cells. MARCH1 overexpression promoted the proliferation, invasion and migration of OS cells. More importantly, MARCH1 overexpression could reverse the tumor inhibition effect mediated by overexpression of miR-486-3p, further demonstrating that MARCH1 was an important target gene for circKEAP1 and miR-486-3p.

It was confirmed that miRNAs could participate in the occurrence and progression of tumors through the secretion of exosomes (47). It was also determined whether extracellular miR-486-3p exerts its roles through incorporating into exosomes.

miR-486-3p could be packed into exosomes and, consistent with its intracellular expression, the exosomal miR-486-3p expression of hFOB cells was higher than that in other OS cell lines. Therefore, exosomes were extracted from derived hFOB cells to conduct co-culture experiments for increased exosomal miR-486-3p expression levels. The proliferation ability of OS cells was suppressed following their treatment with exosomes originating from hFOB cells. These results demonstrated that miR-486-3p could be transmitted between cells through exosomes to inhibit OS cell proliferation.

In conclusion, these data indicated that miR-486-3p was downregulated in OS tissues and cells and acted as a tumor suppressor to impede the malignant behaviors of OS cells. Furthermore, circKEAP1 was highly expressed in OS tissue and cells. Mechanistically, circKEAP1 effectively sponged miR-486-3p, and subsequently increased MARCH1 expression to enhance the malignant behaviors of OS cells. Therefore, the circKEAP1/miR-486-3p/MARCH1 pathway may be critical for regulating the development and progression of OS and may serve as a therapeutic target for OS.

Acknowledgements

Not applicable.

Funding

No funding was received.

Availability of data and materials

The datasets used and/or analyzed during the current study are available from the corresponding author on reasonable request.

Authors' contributions

YF and JJ were the administrators of the present study. HY and CH performed data curation and wrote the manuscript. CH, YF and JJ designed the experiments and analyzed data. HY, CH and YF conducted investigation. CH, YF and JJ confirm the authenticity of all the raw data. HY and JJ reviewed and edited the manuscript. All authors have read and approved the final version of the manuscript.

Ethics approval and consent to participate

Not applicable.

Patient consent for publication

Not applicable.

Competing interests

The authors declare that they have no competing interests.

References

1. Kansara M, Teng MW, Smyth MJ and Thomas DM: Translational biology of osteosarcoma. Nat Rev Cancer 14: 722-735, 2014.
2. Lussier DM, O'Neill L, Nieves LM, McAfee MS, Holechek SA, Collins AW, Dickman P, Jacobsen J, Hingorani P and Blattman JN: Enhanced T-cell immunity to osteosarcoma through antibody blockade of PD-1/PD-L1 interactions. J Immunother 38: 96-106, 2015.
3. Zheng S, Jiang F, Ge D, Tang J, Chen H, Yang J, Yao Y, Yan J, Qiu J, Yin Z, *et al*: LncRNA SNHG3/miRNA-151a-3p/RAB22A axis regulates invasion and migration of osteosarcoma. Biomed Pharmacother 112: 108695, 2019.
4. Awasthi R, Rathbone MJ, Hansbro PM, Bebawy M and Dua K: Therapeutic prospects of microRNAs in cancer treatment through nanotechnology. Drug Deliv Transl Res 8: 97-110, 2018.
5. Lu TX and Rothenberg ME: MicroRNA. J Allergy Clin Immunol 141: 1202-1207, 2018.
6. Petri BJ and Klinge CM: Regulation of breast cancer metastasis signaling by miRNAs. Cancer Metastasis Rev 39: 837-886, 2020.
7. Yang N, Ekanem NR, Sakyi CA and Ray SD: Hepatocellular carcinoma and microRNA: New perspectives on therapeutics and diagnostics. Adv Drug Deliv Rev 81: 62-74, 2015.
8. Konoshenko MY, Bryzgunova OE and Laktionov PP: miRNAs and radiotherapy response in prostate cancer. Andrology 9: 529-545, 2021.
9. Yang Y, Huang Y, Lin W, Liu J, Chen X, Chen C, Yu X and Teng L: Host miRNAs-microbiota interactions in gastric cancer. J Transl Med 20: 52, 2022.
10. Hermansen SK and Kristensen BW: MicroRNA biomarkers in glioblastoma. J Neurooncol 114: 13-23, 2013.
11. Ali Syeda Z, Langden SSS, Munkhzul C, Lee M and Song SJ: Regulatory mechanism of microRNA expression in cancer. Int J Mol Sci 21: 1723, 2020.
12. Fridrichova I and Zmetakova I: MicroRNAs contribute to breast cancer invasiveness. Cells 8: 1361, 2019.
13. He B, Zhao Z, Cai Q, Zhang Y, Zhang P, Shi S, Xie H, Peng X, Yin W, Tao Y and Wang X: miRNA-based biomarkers, therapies, and resistance in cancer. Int J Biol Sci 16: 2628-2647, 2020.
14. Xin X, Kumar V, Lin F, Kumar V, Bhattarai R, Bhatt VR, Tan C and Mahato RI: Redox-responsive nanoplatform for codelivery of miR-519c and gemcitabine for pancreatic cancer therapy. Sci Adv 6: eabd6764, 2020.
15. Ren D, Yang Q, Dai Y, Guo W, Du H, Song L and Peng X: Oncogenic miR-210-3p promotes prostate cancer cell EMT and bone metastasis via NF-κB signaling pathway. Mol Cancer 16: 117, 2017.
16. Tang L, Chen HY, Hao NB, Tang B, Guo H, Yong X, Dong H and Yang SM: microRNA inhibitors: Natural and artificial sequestration of microRNA. Cancer Lett 407: 139-147, 2017.
17. Qi X, Zhang DH, Wu N, Xiao JH, Wang X and Ma W: ceRNA in cancer: Possible functions and clinical implications. J Med Genet 52: 710-718, 2015.
18. Huang G, Liang M, Liu H, Huang J, Li P, Wang C, Zhang Y, Lin Y and Jiang X: CircRNA hsa_circRNA_104348 promotes hepatocellular carcinoma progression through modulating miR-187-3p/RTKN2 axis and activating Wnt/β-catenin pathway. Cell Death Dis 11: 1065, 2020.
19. Zhao M, Feng J and Tang L: Competing endogenous RNAs in lung cancer. Cancer Biol Med 18: 1-20, 2021.
20. Ye J, Li J and Zhao P: Roles of ncRNAs as ceRNAs in gastric cancer. Genes (Basel) 12: 1036, 2021.
21. He Y, Zhou H, Wang W, Xu H and Cheng H: Construction of a circRNA-miRNA-mRNA regulatory network reveals potential mechanism and treatment options for osteosarcoma. Front Genet 12: 632359, 2021.
22. Hill KE, Kelly AD, Kuijjer ML, Barry W, Rattani A, Garbutt CC, Kissick H, Janeway K, Perez-Atayde A, Goldsmith J, *et al*: An imprinted non-coding genomic cluster at 14q32 defines clinically relevant molecular subtypes in osteosarcoma across multiple independent datasets. J Hematol Oncol 10: 107, 2017.
23. Pan Y, Lu L, Chen J, Zhong Y and Dai Z: Identification of potential crucial genes and construction of microRNA-mRNA negative regulatory networks in osteosarcoma. Hereditas 155: 21, 2018.
24. Wang J, Wu Z, Zheng M, Yu S, Zhang X and Xu X: CD146 is closely associated with the prognosis and molecular features of osteosarcoma: Guidance for personalized clinical treatment. Front Genet 13: 1025306, 2022.
25. Han D, Wang M, Yu Z, Yin L, Liu C, Wang J, Liu Y, Jiang S, Ren Z and Yin J: FGF5 promotes osteosarcoma cells proliferation via activating MAPK signaling pathway. Cancer Manag Res 11: 6457-6466, 2019.
26. Diboun I, Wernisch L, Orengo CA and Koltzenburg M: Microarray analysis after RNA amplification can detect pronounced differences in gene expression using limma. BMC Genomics 7: 252, 2006.

27. Varet H, Brillet-Guéguen L, Coppee JY and Dillies MA: SARTools: A DESeq2- and EdgeR-Based R pipeline for comprehensive differential analysis of RNA-Seq data. PLoS One 11: e0157022, 2016.
28. Livak KJ and Schmittgen TD: Analysis of relative gene expression data using real-time quantitative PCR and the 2(-Delta Delta C(T)) method. Methods 25: 402-408, 2001.
29. John B, Enright AJ, Aravin A, Tuschl T, Sander C and Marks DS: Human MicroRNA targets. PLoS Biol 2: e363, 2004.
30. Agarwal V, Bell GW, Nam JW and Bartel DP: Predicting effective microRNA target sites in mammalian mRNAs. Elife 4: e05005, 2015.
31. Wong N and Wang X: miRDB: An online resource for microRNA target prediction and functional annotations. Nucleic Acids Res 43: D146-D152, 2015.
32. Betel D, Wilson M, Gabow A, Marks DS and Sander C: The microRNA.org resource: Targets and expression. Nucleic Acids Res 36: D149-D153, 2008.
33. Chen C, Xie L, Ren T, Huang Y, Xu J and Guo W: Immunotherapy for osteosarcoma: Fundamental mechanism, rationale, and recent breakthroughs. Cancer Lett 500: 1-10, 2021.
34. Li X, Ding J, Wang X, Cheng Z and Zhu Q: NUDT21 regulates circRNA cyclization and ceRNA crosstalk in hepatocellular carcinoma. Oncogene 39: 891-904, 2020.
35. Xu N, Yang W, Liu Y, Yan F and Yu Z: MicroRNA-411 promoted the osteosarcoma progression by suppressing MTSS1 expression. Environ Sci Pollut Res Int 25: 12064-12071, 2018.
36. Lee YS and Dutta A: MicroRNAs in cancer. Annu Rev Pathol 4: 199-227, 2009.
37. Chan JJ and Tay Y: Noncoding RNA: RNA regulatory networks in cancer. Int J Mol Sci 19: 1310, 2018.
38. Misir S, Hepokur C, Aliyazicioglu Y and Enguita FJ: Circular RNAs serve as miRNA sponges in breast cancer. Breast Cancer 27: 1048-1057, 2020.
39. He M, Wang G, Jiang L, Qiu C, Li B, Wang J and Fu Y: miR-486 suppresses the development of osteosarcoma by regulating PKC-δ pathway. Int J Oncol 50: 1590-1600, 2017.
40. Liu Y, Zhang J, Xing C, Wei S, Guo N and Wang Y: miR-486 inhibited osteosarcoma cells invasion and epithelial-mesenchymal transition by targeting PIM1. Cancer Biomark 23: 269-277, 2018.
41. Namløs HM, Skårn M, Ahmed D, Grad I, Andresen K, Kresse SH, Munthe E, Serra M, Scotlandi K, Llombart-Bosch A, *et al*: miR-486-5p expression is regulated by DNA methylation in osteosarcoma. BMC Genomics 23: 142, 2022.
42. Wu J, Xia L, Yao X, Yu X, Tumas KC, Sun W, Cheng Y, He X, Peng YC, Singh BK, *et al*: The E3 ubiquitin ligase MARCH1 regulates antimalaria immunity through interferon signaling and T cell activation. Proc Natl Acad Sci USA 117: 16567-16578, 2020.
43. Meng Y, Hu J, Chen Y, Yu T and Hu L: Silencing MARCH1 suppresses proliferation, migration and invasion of ovarian cancer SKOV3 cells via downregulation of NF-κB and Wnt/β-catenin pathways. Oncol Rep 36: 2463-2470, 2016.
44. Yang W, Su J, Li M, Li T, Wang X, Zhao M and Hu X: Myricetin induces autophagy and cell cycle arrest of HCC by inhibiting MARCH1-regulated Stat3 and p38 MAPK signaling pathways. Front Pharmacol 12: 709526, 2021.
45. Wang N, Yang L, Dai J, Wu Y, Zhang R, Jia X and Liu C: 5-FU inhibits migration and invasion of CRC cells through PI3K/AKT pathway regulated by MARCH1. Cell Biol Int 45: 368-381, 2021.
46. Su Y, Feng W, Zhong G, Ya Y, Du Z, Shi J, Chen L, Dong W and Lin T: ciRs-6 upregulates March1 to suppress bladder cancer growth by sponging miR-653. Aging (Albany NY) 11: 11202-11223, 2019.
47. Boelens MC, Wu TJ, Nabet BY, Xu B, Qiu Y, Yoon T, Azzam DJ, Twyman-Saint Victor C, Wiemann BZ, Ishwaran H, *et al*: Exosome transfer from stromal to breast cancer cells regulates therapy resistance pathways. Cell 159: 499-513, 2014.